Applied Aerodynamics 3

Roi Baruch, ID 211914866

August 23, 2024

Contents

List of Figures

A Part A

A.1

The Thwaites' method can be used to solve a laminar boundary layer over a flat flat. Looking at various inverted boundary layer profiles in Figure 1, it can be seen that the steeper the gradient of the velocity profile, the "healthier" the boundary layer is. As the flow reaches closer to the transition, the gradient decreases.

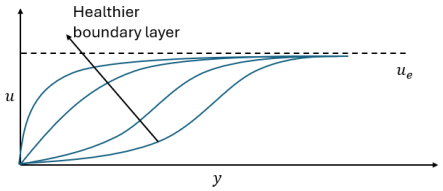

Figure 1: Inverted laminar boundary layer profile

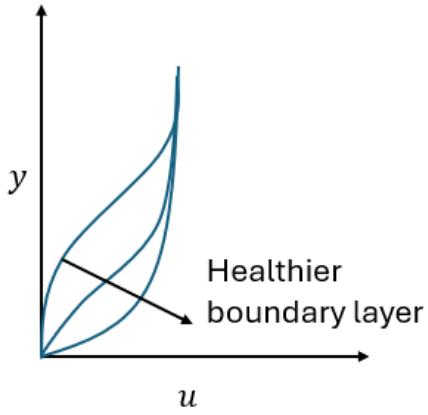

Figure 2: Laminar boundary layer profile

Now, looking at the two following expressions $\left.\frac{\partial u}{\partial y}\right|_w$ and $\left.\frac{\partial^2 u}{\partial y^2}\right|_w$, they can be expressed with the velocity scale u_e and length scale θ as follows:

$$\left.\frac{\partial u}{\partial y}\right|_w \propto \frac{u_e}{\theta} = \frac{u_e}{\theta} l \tag{1}$$

Where l is an unknown scalar. For the second derivative:

$$\left.\frac{\partial^2 u}{\partial y^2}\right|_w \propto -\frac{u_e}{\theta} = -\frac{u_e}{\theta^2}\lambda \tag{2}$$

Where θ is also an unknown scalar. Looking at the second derivative in Figure 1, it can be seen that a healthier boundary layer corresponds to bigger λ values as the gradient absolute value near the wall increases. Using the momentum equation for the boundary layer, λ can be found:

$$u\frac{\partial u}{\partial x} + v\frac{\partial u}{\partial y} = u_e\frac{du_e}{dx} + \nu\frac{\partial^2 u}{\partial y^2} \tag{3}$$

looking at the wall, imposing no-slip conditions $u = v = 0$ and substituting in 2

$$\cancel{u\frac{\partial u}{\partial x}} + \cancel{v\frac{\partial u}{\partial y}} = u_e\frac{du_e}{dx} + \nu\frac{\partial^2 u}{\partial y^2}\bigg|_w \tag{4}$$

$$0 = \cancel{u_e}\frac{du_e}{dx} - \nu\frac{\cancel{u_e}}{\theta^2}\lambda \tag{5}$$

$$\lambda = \frac{\theta^2}{\nu}\frac{du_e}{dx} \tag{6}$$

Now looking at the von Kármán Momentum Integral Equation:

$$\frac{1}{2}c_f = \frac{\theta}{u_e}(H+2)\frac{du_e}{dx} + \frac{d\theta}{dx} \tag{7}$$

Searching for a connection between the skin friction coefficient and the problem variables u_e and θ:

$$c_f = \frac{\tau_w}{\frac{1}{2}\rho u_e^2} \tag{8}$$

$$\tau_w = \mu\left.\frac{du}{dy}\right|_w \tag{9}$$

Using 8 and 9 and the definition for kinematic viscosity $\nu = \frac{\mu}{\rho}$ the following connection can be obtained:

$$c_f = \frac{\mu\left.\frac{du}{dy}\right|_w}{\frac{1}{2}\rho u_e^2} \tag{10}$$

Substituting in 1

$$c_f = \frac{2\nu}{u_e^2}\frac{u_e}{\theta}l = \frac{2\nu l}{u_e\theta} \tag{11}$$

Rearranging 6 as:

$$\frac{du_e}{dx} = \frac{\lambda\nu}{\theta^2} \tag{12}$$

Substituting 11 and 12 back to 7:

$$\frac{\nu l}{u_e\theta} = \frac{d\theta}{dx} + \frac{1}{u_e}(H+2)\frac{\nu\lambda}{\theta} \tag{13}$$

Rearranging all the unknowns to the LHS:

$$\frac{d\theta}{dx} = \frac{\nu l}{u_e\theta} - \frac{1}{u_e}(H+2)\frac{\nu\lambda}{\theta} \tag{14}$$

$$\frac{d\theta}{dx} = \frac{\nu}{u_e\theta}(l - \lambda(H+2)) \tag{15}$$

$$\frac{u_e\theta}{\nu}\frac{d\theta}{dx} = l - \lambda(H+2) \tag{16}$$

The RHS of 16 can be expressed as a linear function of λ from experimental:

$$l - \lambda(H+2) \equiv 0.225 - 3\lambda \tag{17}$$

Substituting back into 16 an ODE for θ can be obtained:

$$\frac{u_e\theta}{\nu}\frac{d\theta}{dx} = 0.225 - 3\lambda \tag{18}$$

Or

$$\frac{d\theta}{dx} = 0.225\frac{\nu}{u_e\theta} - 3\lambda\frac{\nu}{u_e\theta} \tag{19}$$

Using 6

$$\frac{d\theta}{dx} = 0.225\frac{\nu}{u_e\theta} - 3\frac{\theta^{\cancel{2}}}{\cancel{\nu}}\frac{du_e}{dx}\frac{\cancel{\nu}}{u_e\cancel{\theta}} \tag{20}$$

$$\frac{d\theta}{dx} = 0.225\frac{\nu}{u_e\theta} - \frac{3\theta}{u_e}\frac{du_e}{dx} \tag{21}$$

The Solution procedure includes:

1. solving the ODE for θ as shown in 21
2. Computing λ as shown in 6 to check for transition
3. competing, H using the following data fits:

$$\begin{cases} l = 0.22 + 1.57\lambda - 1.8\lambda^2 \\ H = 2.61 - 3.75\lambda - 5.24\lambda^2 \end{cases} \quad \text{if } 0 \le \lambda \le 0.1 \tag{22}$$

$$\begin{cases} l = 0.22 + 1.402\lambda + \frac{0.018\lambda}{0.107+\lambda} \\ H = 2.088 + \frac{0.0731}{0.14+\lambda} \end{cases} \quad \text{if } -0.1 < \lambda < 0 \tag{23}$$

4. Computing the displacement thickness $\delta^* = H\theta$
5. Compute the local skin friction coefficient $c_f = \frac{2\nu l}{u_e\theta}$

With the initial conditions for a flat plate being (starting from $x_0 = 10^-6$)

$$\theta_0 = \frac{0.664x_0}{\sqrt{Re_{x_0}}} \tag{24}$$

Or for an airfoil

$$\theta_0 = \left[\frac{0.075\nu}{(\frac{du_e}{dx})_0}\right]^{0.5} \tag{25}$$

Implementing the Thwaites method for a flat plate with a laminar boundary layer, plotting and comparing to the analytical Blasius solution:

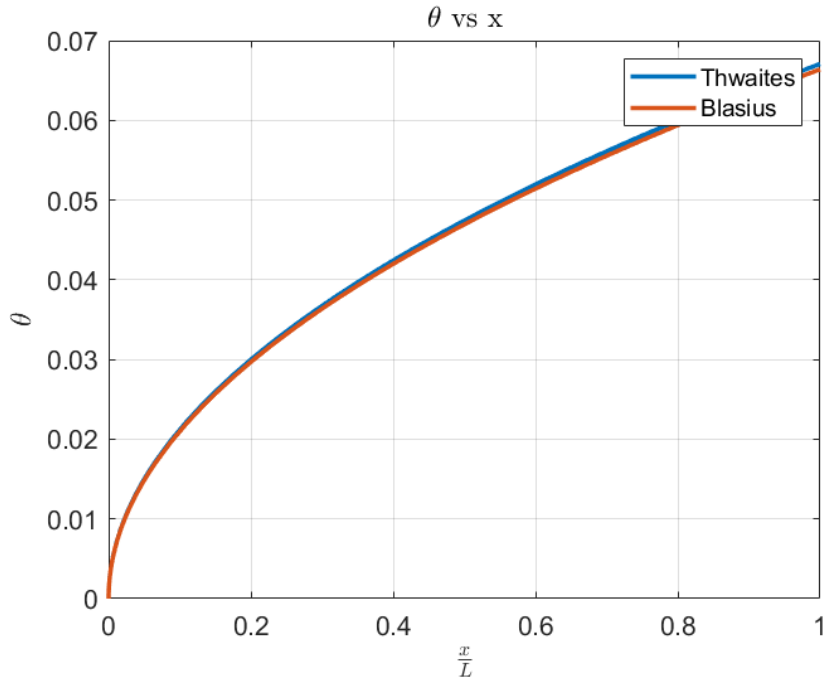

Figure 3: θ vs $\frac{x}{L}$ for a laminar boundary layer

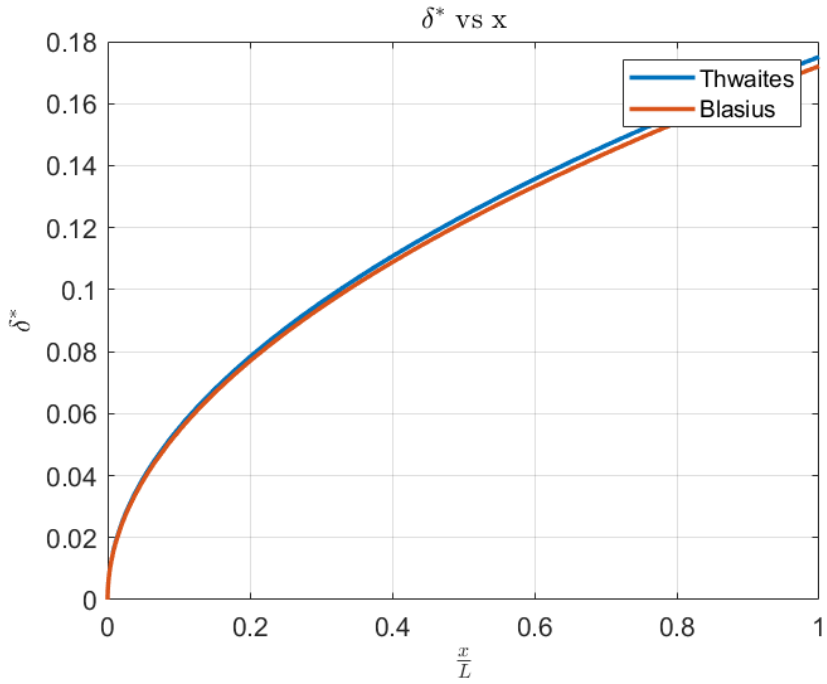

Figure 4: δ^* vs $\frac{x}{L}$ for a laminar boundary layer

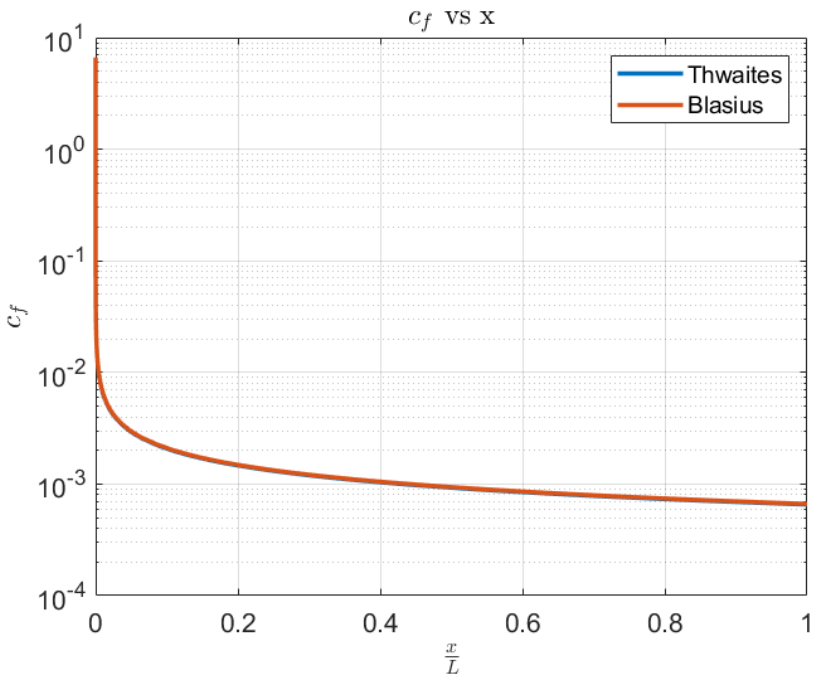

Figure 5: c_f vs $\frac{x}{L}$ for a laminar boundary layer

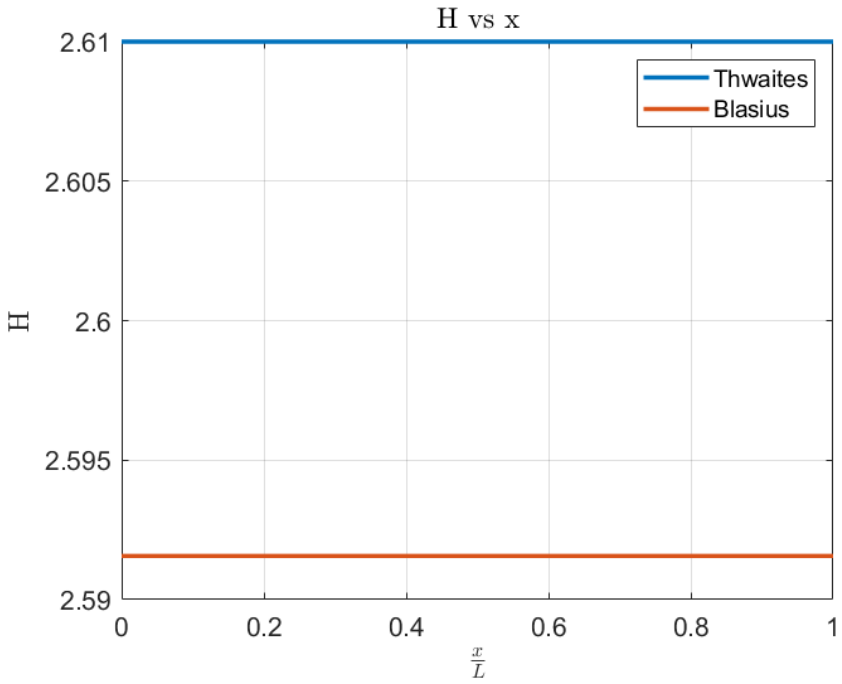

Figure 6: H vs $\frac{x}{L}$ for a laminar boundary layer

As seen in the figures above, the numerical solution for the Thwaites method and the analytical Blasius solution are nearly identical, noticing in figure 6 the difference between the H values is ≈ 0.02. The Total values for C_f are both $C_f = 0.0013$.

A.2

Taking a small element of the turbulent boundary layer, a mass conservation equation can be written:

$$\int \rho \overline{u} \cdot d\overline{a} = 0 \tag{26}$$

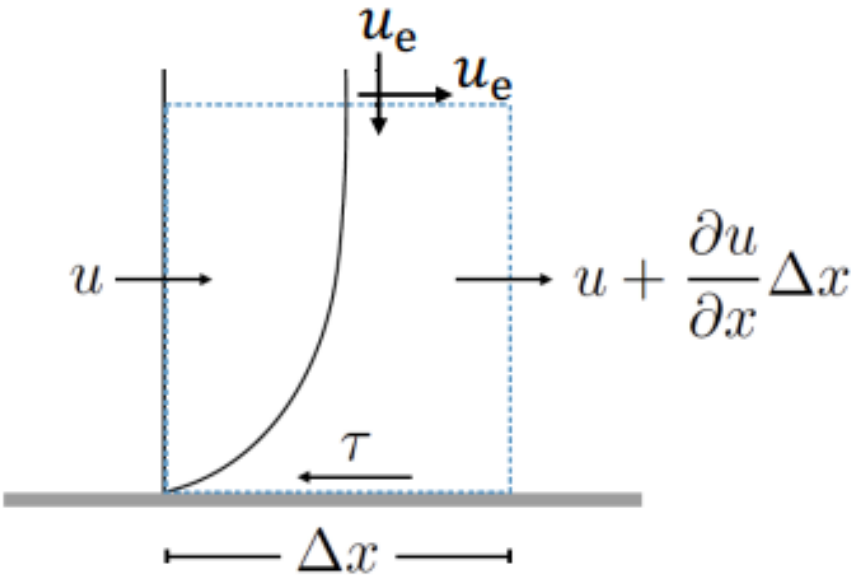

Figure 7: turbulent boundary layer CV

Taking the mass conservation equation on the CV from figure 7

$$-\int_0^\delta \cancel{\rho u} dy + \int_0^\delta (\cancel{\rho u} + \frac{\partial(\cancel{\rho} u)}{\partial x}\cancel{\Delta x})dy - \cancel{\rho} v_e \cancel{\Delta x} = 0 \tag{27}$$

Getting

$$v_e = \int_0^\delta \frac{\partial u}{\partial x} dy \tag{28}$$

Where v_e is the velocity that is pulled into the CV. Head assumed that the normalized entrainment velocity v_e was self-similar with the mean velocity profile, namely with H:

$$\frac{v_e}{u_e} = f(H) \tag{29}$$

Thus, for the BL is

$$\frac{v_e}{u_e} = \frac{1}{u_e}\int_0^\delta \frac{\partial u}{\partial x} dy = f(H) \tag{30}$$

$$\int_0^\delta \frac{\partial u}{\partial x} dy = u_e f(H) \tag{31}$$

Taking out the derivative

$$\frac{\partial}{\partial x}\int_0^\delta u dy = u_e f(H) \tag{32}$$

$$\frac{\partial}{\partial x}\int_0^\delta (u_e - u_e + u) dy = u_e f(H) \tag{33}$$

$$\frac{\partial}{\partial x}\int_0^{\delta} u_e(1-(1-\frac{u}{u_e}))dy = u_e f(H) \tag{34}$$

Knowing that

$$\delta^* = \int_0^{\infty}(1-\frac{u}{u_e})dy \tag{35}$$

The equation can be rearranged, such as

$$\frac{\partial}{\partial x}\int_0^{\delta} u_e(1-(1-\frac{u}{u_e}))dy = \frac{\partial}{\partial x}u_e\left[\int_0^{\delta} 1dy - \int_0^{\delta}(1-\frac{u}{u_e}))dy\right] \tag{36}$$

$$\frac{d}{dx}(u_e(\delta-\delta^*)) = u_e f(H) \tag{37}$$

Defining a new variable $H_1 = \frac{\delta-\delta^*}{\theta}$ and Substituting into the equation

$$\frac{d}{dx}(u_e H\theta) = u_e f(H) \tag{38}$$

Head found an experimental relationship for $f(H)$ and between H_1 and H:

$$f(H) = 0.0306(H_1-3)^{-0.6169} \tag{39}$$

$$H_1 = \begin{cases} 0.8234(H-1.1)^{-1.287}+3.3 & \text{for } H \leq 1.6 \\ 1.5501(H-0.6778)^{-3.064}+3.3 & \text{for } H > 1.6 \end{cases} \tag{40}$$

Using the chain rule for equation 38

$$\frac{d}{dx}\left(u_e H_1\theta\right) = H_1\theta\frac{du_e}{dx} + H_1 u_e\frac{d\theta}{dx} + u_e\theta\frac{dH_1}{dx} = u_e 0.0306\left(H_1-3\right)^{-0.6169} \tag{41}$$

Rearranging it as an ODE for H_1

$$\frac{dH_1}{dx} = \frac{0.0306}{\theta}\left(H_1-3\right)^{-0.6169} - \frac{H_1}{u_e}\frac{du_e}{dx} - \frac{H_1}{\theta}\frac{d\theta}{dx} \tag{42}$$

Using the Momentum Integral Equation from equation 7 and rearranging it as an ODE for θ

$$\frac{d\theta}{dx} = \frac{1}{2}c_f - \frac{\theta}{u_e}(H+2)\frac{du_e}{dx} \tag{43}$$

Now, the two coupled ODEs are:

$$\begin{cases} \frac{dH_1}{dx} = \frac{0.0306}{\theta}\left(H_1-3\right)^{-0.6169} - \frac{H_1}{u_e}\frac{du_e}{dx} - \frac{H_1}{\theta}\frac{d\theta}{dx} & (I) \\ \frac{d\theta}{dx} = \frac{1}{2}c_f - \frac{\theta}{u_e}(H+2)\frac{du_e}{dx} & (II) \end{cases} \tag{44}$$

We have $H_1 = f(H)$, but we need its inverse $H = f(H_1)$, given below:

$$H = \begin{cases} 3.0 & \text{for } H_1 \leq 3.3 \\ 1.1538(H_1-3.3)^{-0.326}+0.6778 & \text{for } 3.3 < H_1 \leq 5.3 \\ 0.86(H_1-3.3)^{-0.777}+1.1 & \text{for } H_1 \geq 5.3 \end{cases} \tag{45}$$

The skin friction coefficient can be estimated using the following semi-empirical formula:

$$c_f = 0.246 \times 10^{-0.678H} Re_\theta^{-0.268} \tag{46}$$

With

$$Re_\theta = \frac{u_e \theta}{\nu} \tag{47}$$

The Solution procedure includes:

1. Solving the two ODEs for θ and H_1
2. Evaluate H
3. Compute the local skin friction coefficient C_f

With the initial conditions being

$$\theta_0 = \theta_{laminar_{final}} \tag{48}$$

And

$$H_0 = 1.28 \rightarrow H_1 = 10.6 \tag{49}$$

Separation is defined as $C_f \rightarrow 0$, which happens at a typical value of $H = 3$. Implementing the Head method for a flat plate with a turbulent boundary layer from the start, plotting and comparing to the empirical Schlichting formulas:

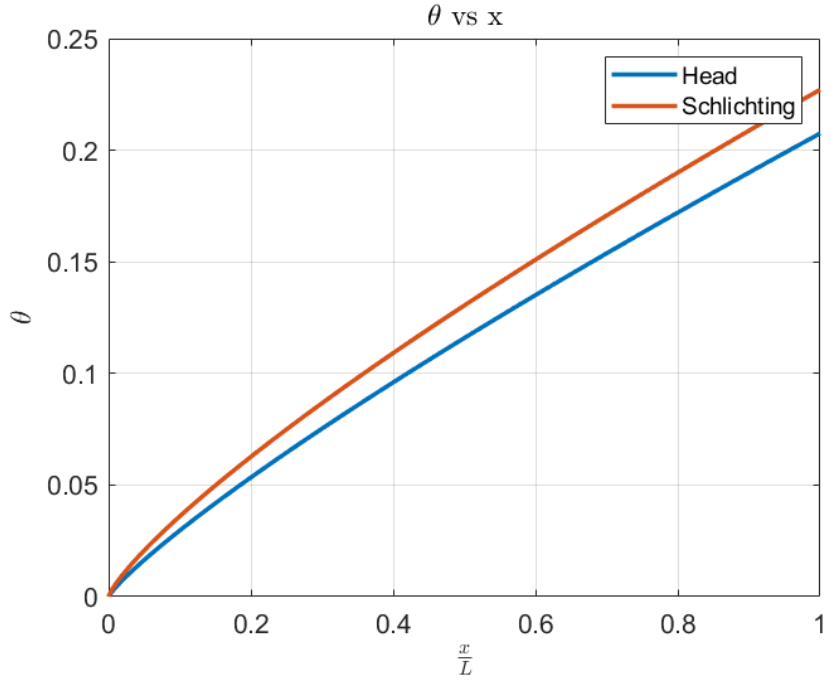

Figure 8: θ vs $\frac{x}{L}$ for a turbulent boundary layer

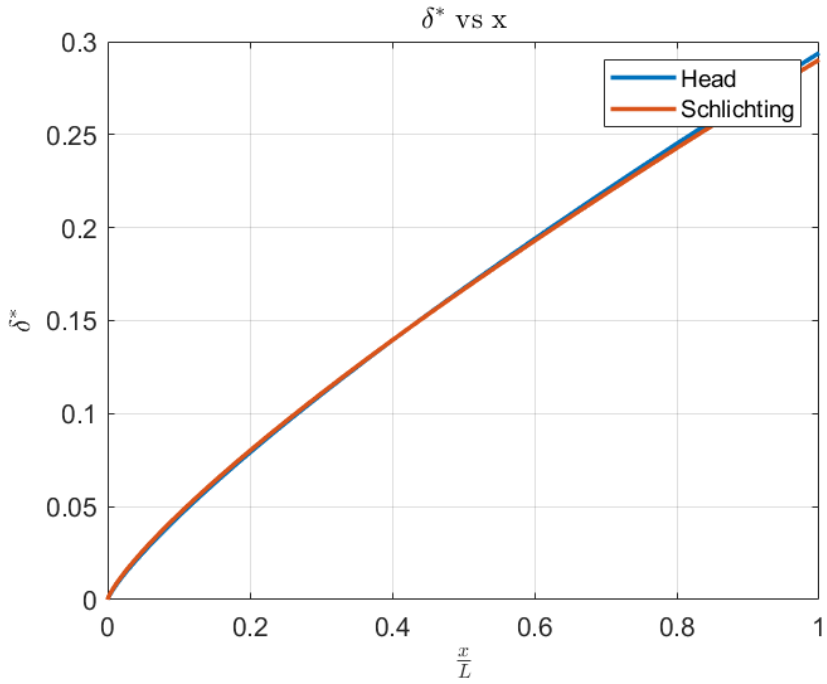

Figure 9: δ^* vs $\frac{x}{L}$ for a turbulent boundary layer

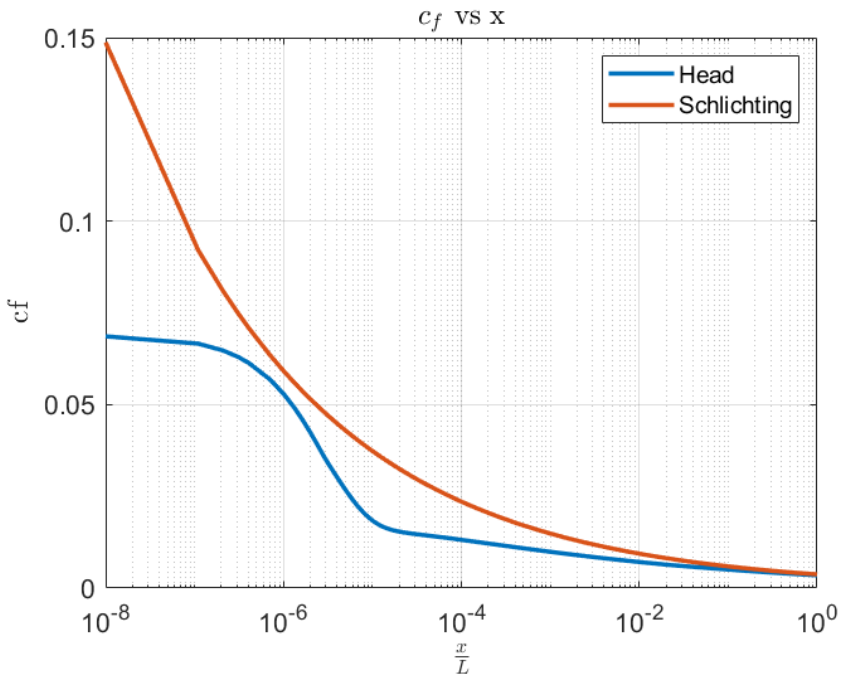

Figure 10: c_f vs $\frac{x}{L}$ for a turbulent boundary layer

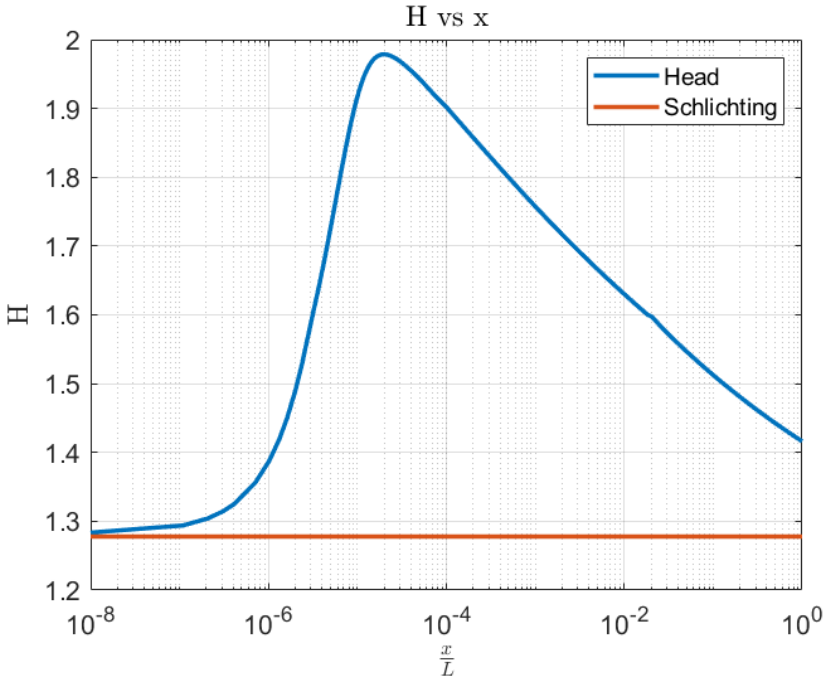

Figure 11: H vs $\frac{x}{L}$ for a turbulent boundary layer

The figures above show that the Head method solution closely resembles the empirical Schlichting formulas. In figure 8, the solution differs from the empirical formulas more than in the laminar case, as seen in figure 3. This difference results from the turbulent boundary layer being much more difficult to predict. In figure 11, the H value for the Head method increases at the very beginning of the plate due to the boundary layer being "tripped" and starting from a turbulent state. The Schlichting empirical solution is constant through the plate at a value of ≈ 1.28. The total skin coefficient for Schlichting is $C_{f_{sch}} = 0.0047$, $C_{f_{Head}} = 0.0042$.

B Part B

A complete viscus solution using panel methods will be made in part B. Using the Hess-Smith method for the inviscid solution and solving the boundary layer with the method shown in Part A.

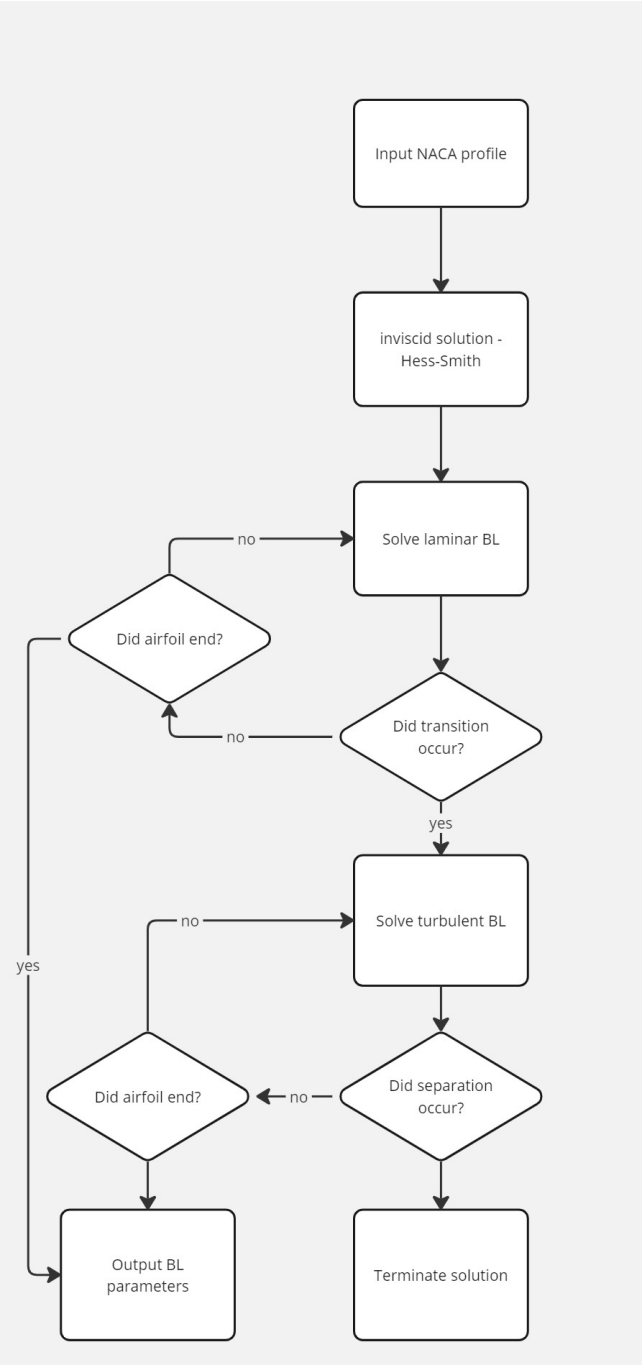

Figure 12: Solution procedure flowchart

Michel's method is used to detect the transition point on the upper and lower surfaces of the airfoil using the local Reynolds number:

$$Re_x = \frac{u_e x}{\nu} \tag{50}$$

And the Reynolds number using the momentum thickness

$$Re_\theta = \frac{u_e \theta}{\nu} \tag{51}$$

for airfoil-type applications, the transition should be expected when:

$$Re_\theta > 1.174(1 + \frac{22400}{Re_x})Re_x^{0.46} \tag{52}$$

After the transition is detected, the boundary layer solution is updated to the turbulent solver from the next panel. Separation is detected when $H = 3$; after that, the solution is terminated due to the panel method not being valid for a separated flow.

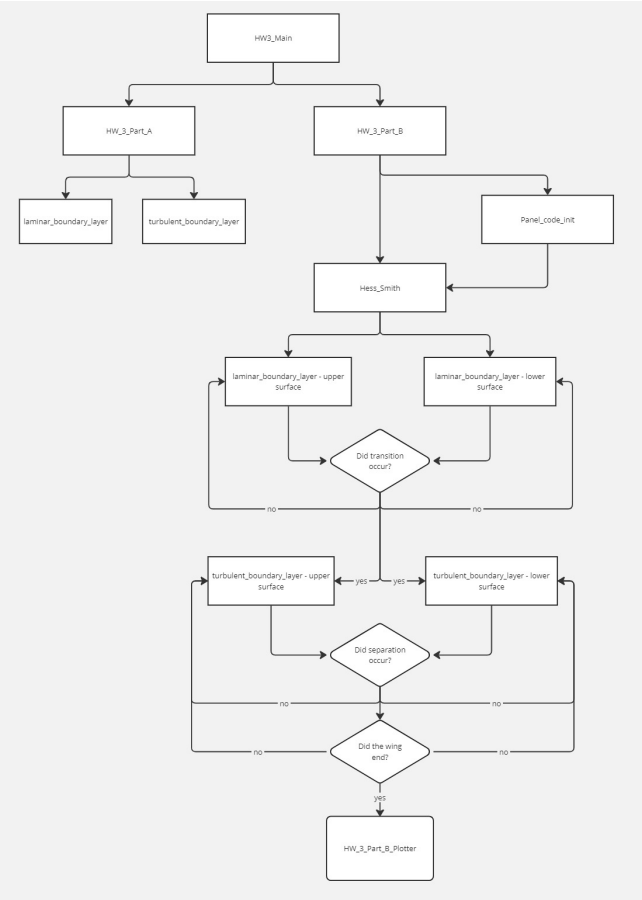

Figure 13: Functions flowchart

B.1

For an angle of attack of 5°, computing and plotting δ^*, θ, c_f, H vs. distance from the leading edge stagnation point for both the upper and lower surface boundary layers:

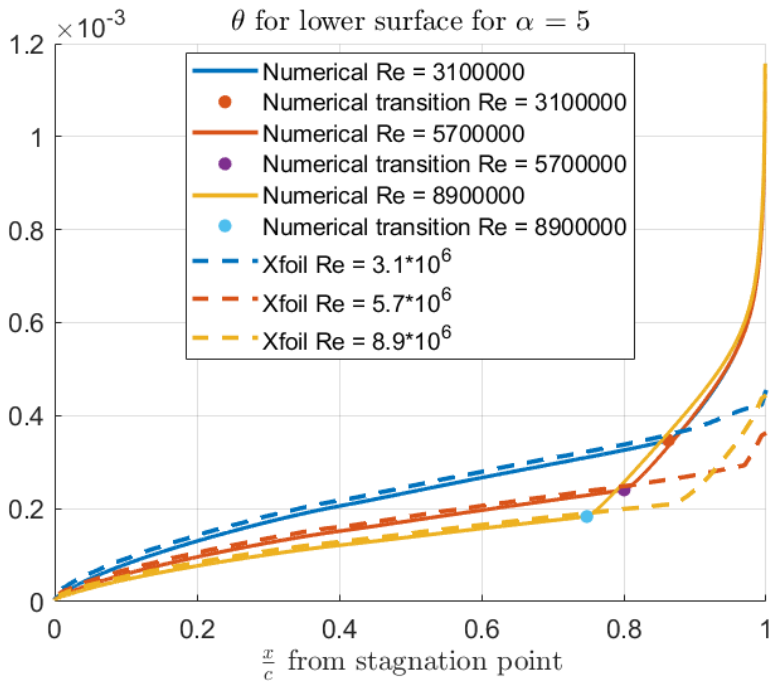

Figure 14: θ lower surface

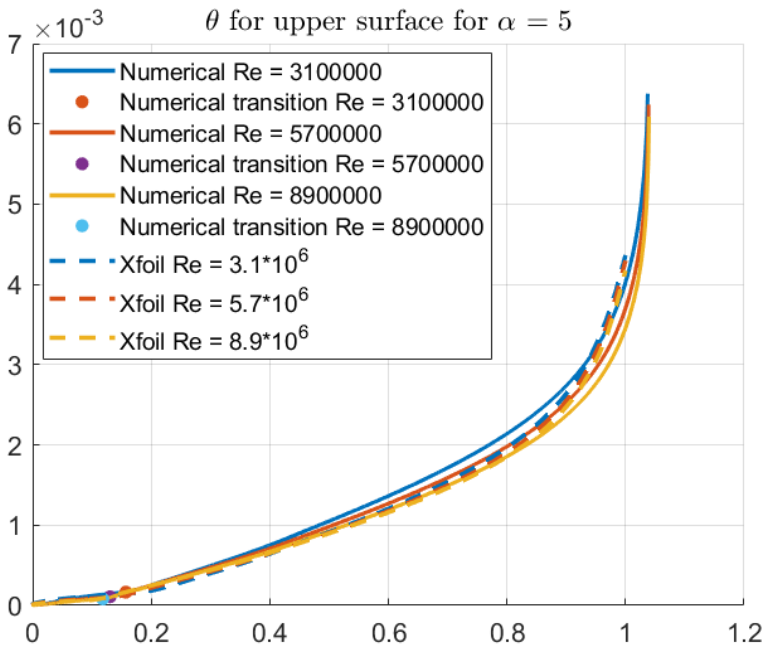

Figure 15: θ upper surface

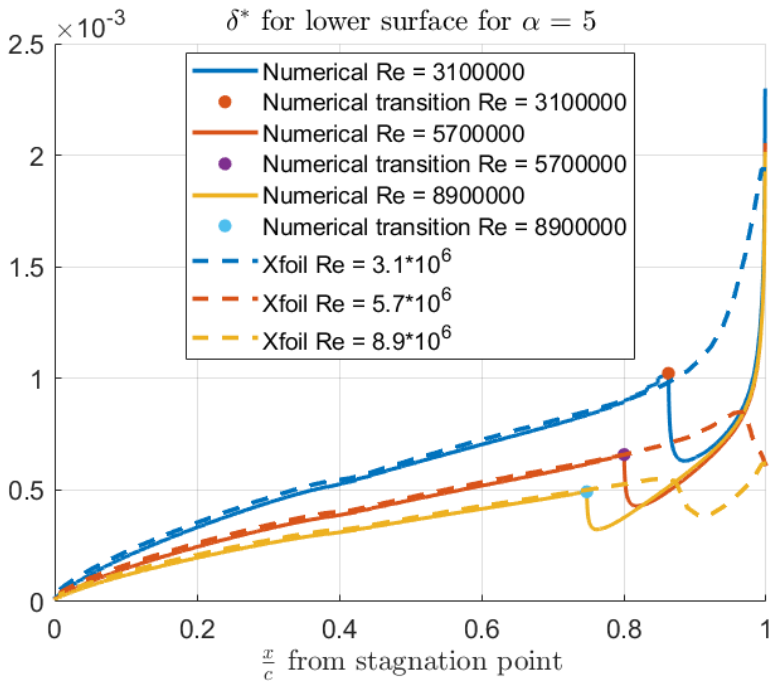

Figure 16: δ^* lower surface

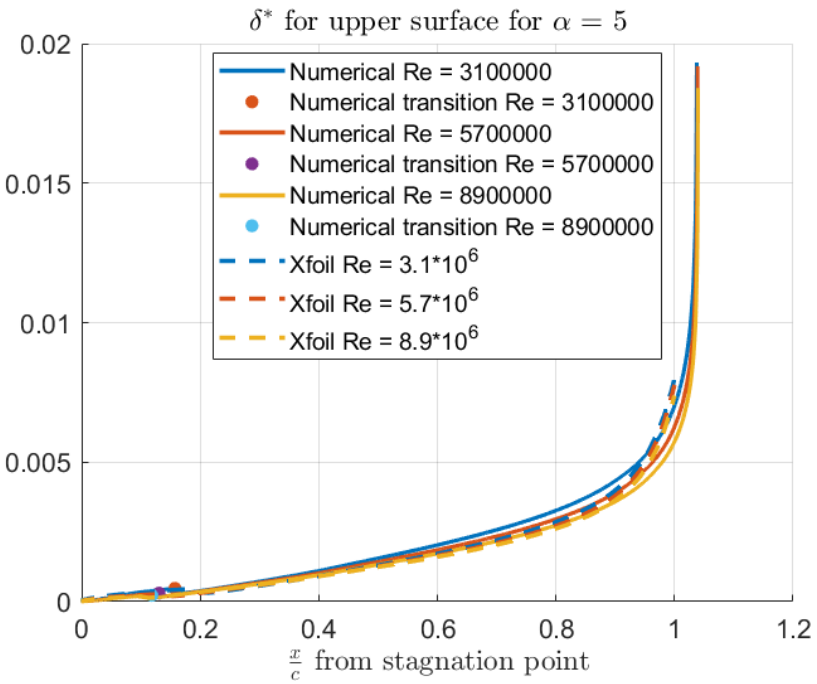

Figure 17: δ^* upper surface

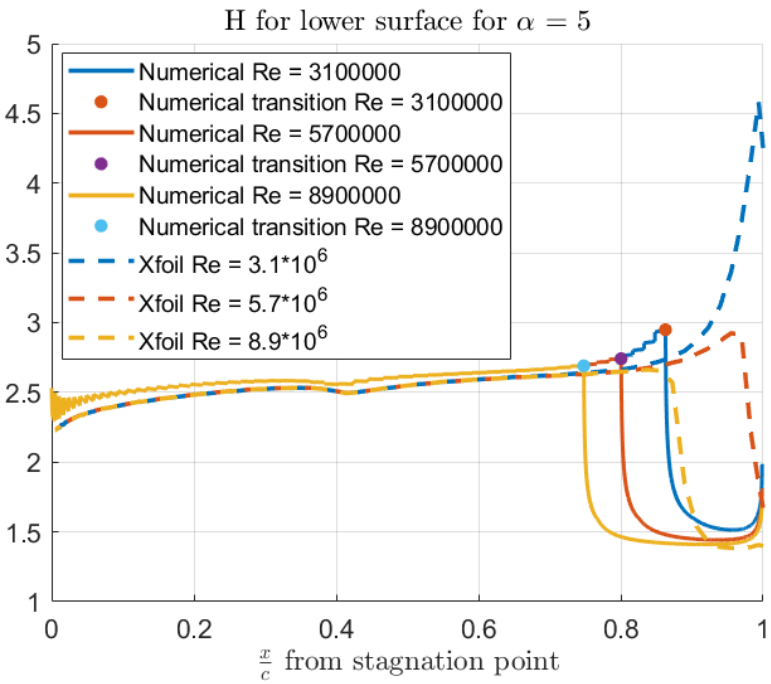

Figure 18: H lower surface

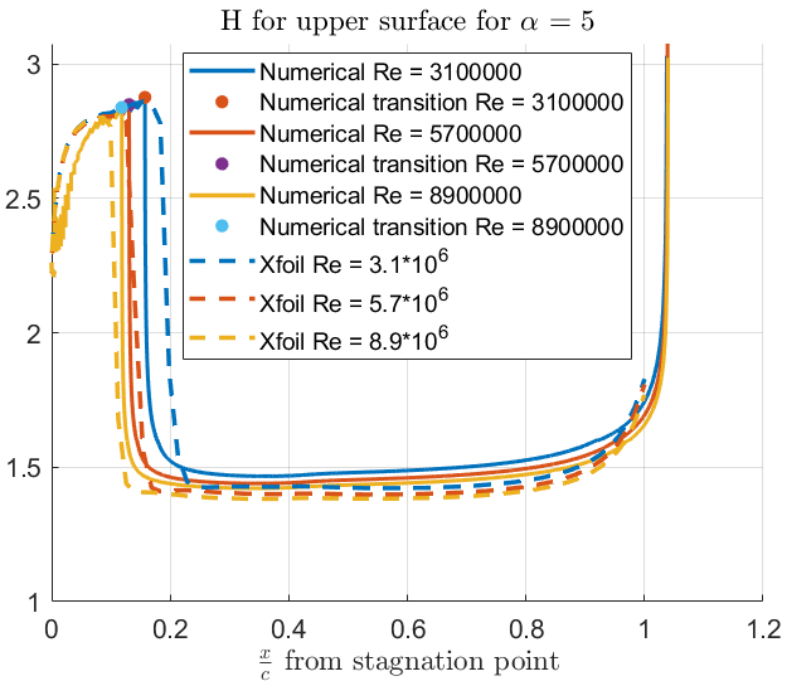

Figure 19: H upper surface

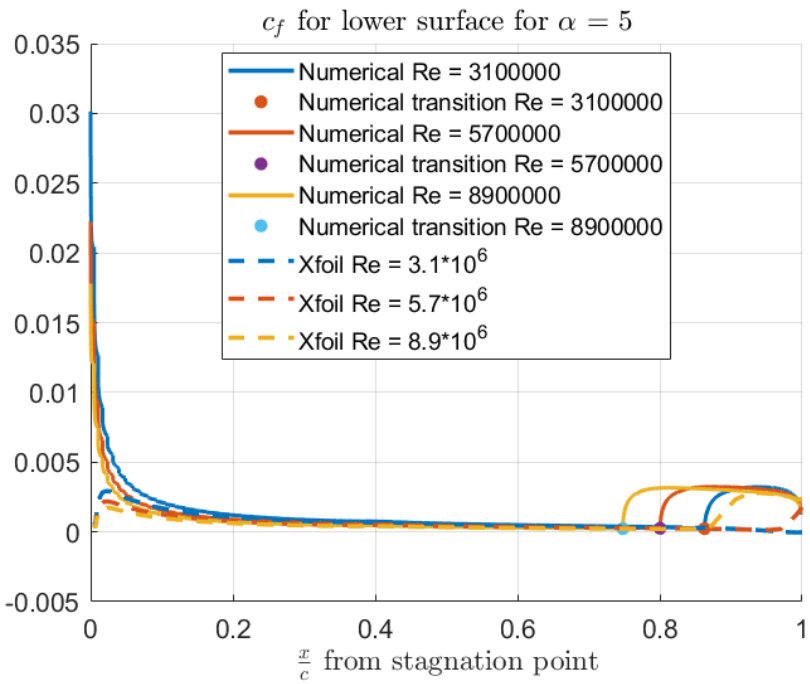

Figure 20: c_f lower surface

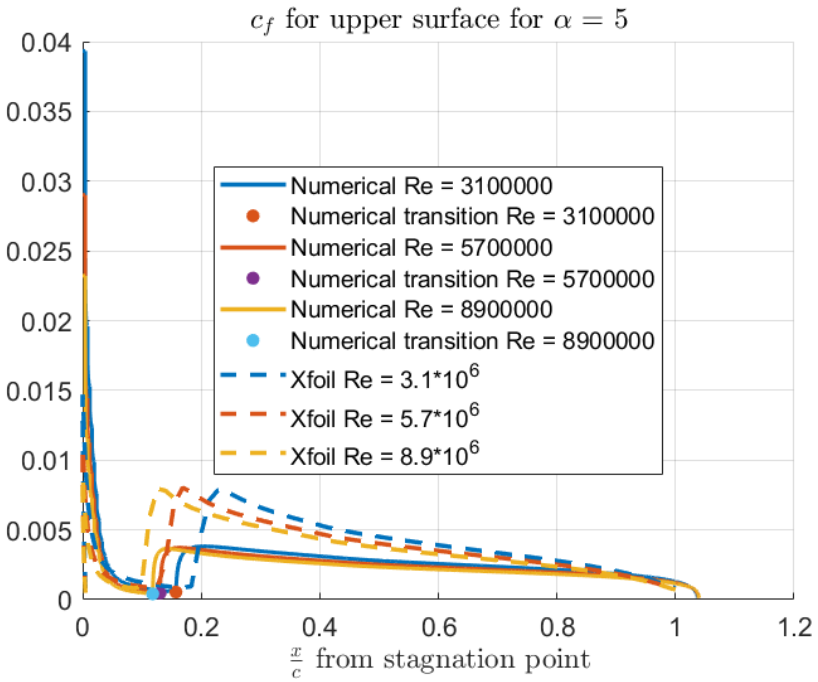

Figure 21: c_f upper surface

Observing the plots for all the boundary layer parameters for the NACA 2412 at $\alpha = 5°$. Looking at the upper surface, the transition can be observed in figure 19 when the H values drop as the flow transitions to a turbulent state. Separation is detected at the last panel of the upper surface in the panel code when $H = 3$.

	$Re = 3.1 \times 10^6$	$Re = 5.7 \times 10^6$	$Re = 8.9 \times 10^6$
Xfoil	0.1828	0.1324	0.0994
Panel code	0.1573	0.1307	0.1183

Table 1: $\frac{x}{c}$ transition point from the stagnation point - Upper surface

Differences in the location of the transition point between the panel code and Xfoil can be a result of a few different factors:

1. Different inviscid panel methods
2. Xfoil solves the boundary layer and updates the solution for multiple iterations while the panel only does a single iteration.
3. Xfoil detects the transition point using $H - Re_x$ with e^N method, while the panel code uses Michel's method as seen in equation 52.

The transition is detected much later on the lower surface, as seen in 18, and the flow isn't separated.

	$Re = 3.1 \times 10^6$	$Re = 5.7 \times 10^6$	$Re = 8.9 \times 10^6$
Panel code	0.8627	0.8004	0.7480
Xfoil	0.9976	0.9694	0.8698

Table 2: $\frac{x}{c}$ transition point from the stagnation point - Lower surface

Looking at the transition point at the lower surface, a bigger gap can be observed between the panel code and Xfoil. This difference can result from a more "energetic" boundary layer with higher H values from the stagnation point. Another observation looking at the H graph are the discontinuities. Since a constant u_e for each panel was assumed, the derivative will be a non-continuous function. This discontinuity carries over to the λ values, resulting in a non-continuous H graph. An earlier stagnation point for higher Reynolds numbers is a general trend for the upper and lower surface. Figures 20 and 21 show that when the flow reaches transition or separation, the value of the skin friction coefficient reaches zero: $c_f \to 0$.

B.2

Computing the drag coefficient of the airfoil at an angle of attack of 5° using the Squire-Young :

$$C_d = \frac{2\theta_{TE}}{c}(\frac{u_{e_{TE}}}{V_\infty})^{\frac{H_{TE}+5}{2}} \tag{53}$$

Combine both the upper and lower surfaces to create a total drag coefficient. And comparing it to published data:

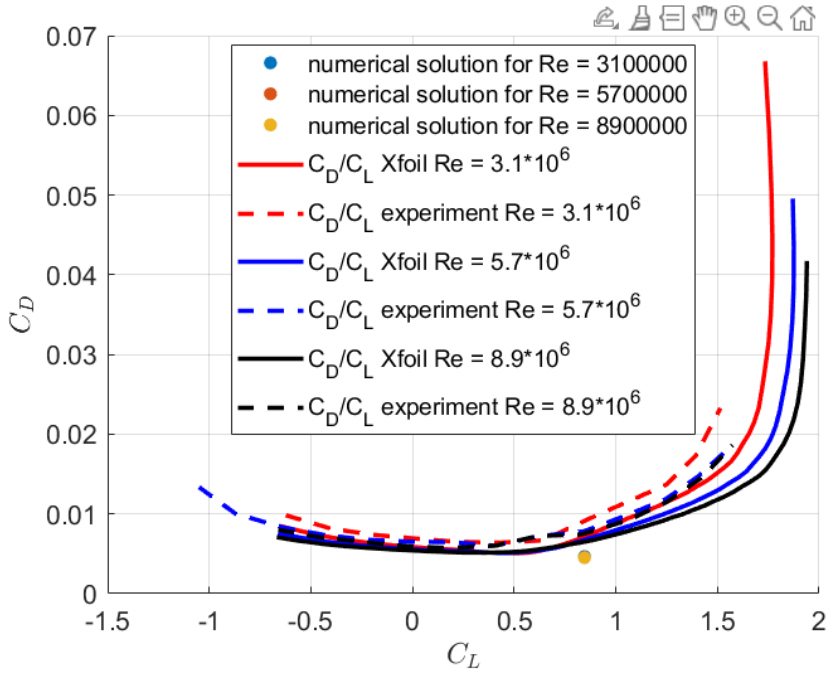

Figure 22: C_D vs C_L

	Xfoil	Panel code	NACA 1945
$Re = 3.1 \times 10^6$	0.0070	0.0046	0.0080
$Re = 5.7 \times 10^6$	0.0067	0.0045	0.0076
$Re = 8.9 \times 10^6$	0.0065	0.0045	0.0074

Table 3: C_D

The drag coefficient from the panel code, which considers the viscous effects, differs from the experimental data by as much as almost twice. The drag computed by Xfoil still differs from the experimental data but much less than the panel code.

B.3

Predicting the maximum lift coefficient $C_{L_{max}}$, using the panel code when the transition is forced at $\frac{x}{c} = 0.01$ on the upper surface. The angle of attack when the maximum lift coefficient will be obtained is when the separation on the upper surface will happen at $\frac{x}{c} = 0.85$.

α	x_{tran}	C_L
14°	0.915c	1.902
15°	0.861c	2.016
16°	0.789c	2.131

Table 4: $C_{l_{max}}$

Thus α at which $C_{l_{max}}$ is achieved is 15°.

B.4

constructing as much of the drag polar of the airfoil at the three corresponding Reynolds numbers:

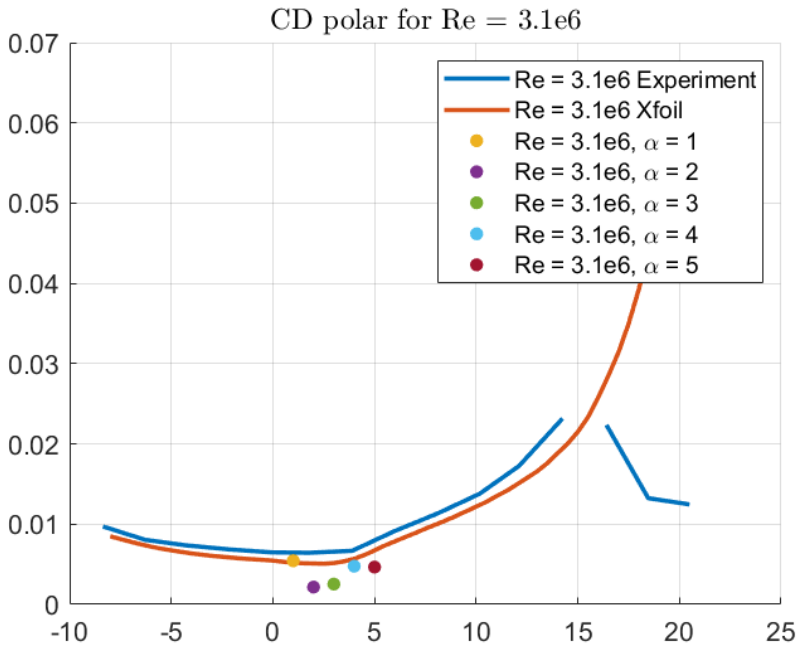

Figure 23: C_d polar for $Re = 3.1 \times 10^6$

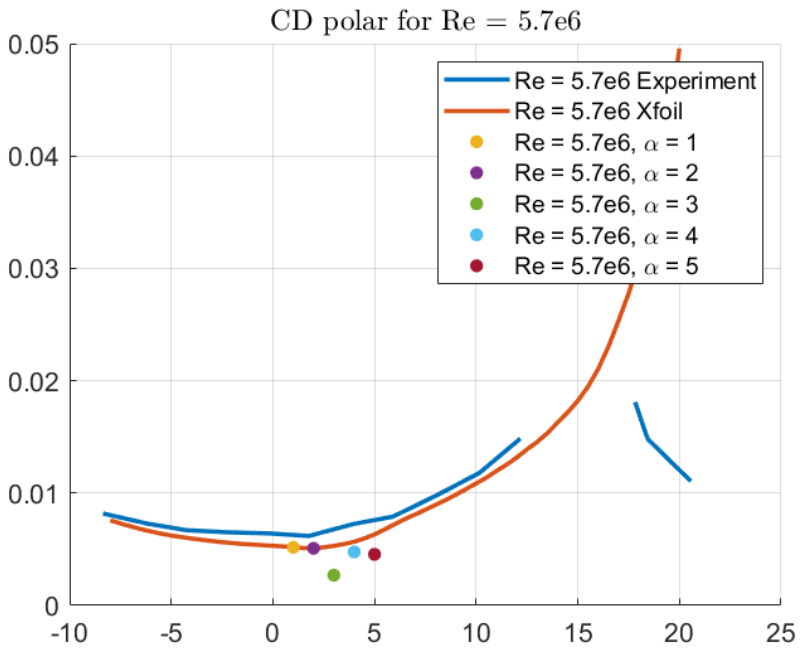

Figure 24: C_d polar for $Re = 5.7 \times 10^6$

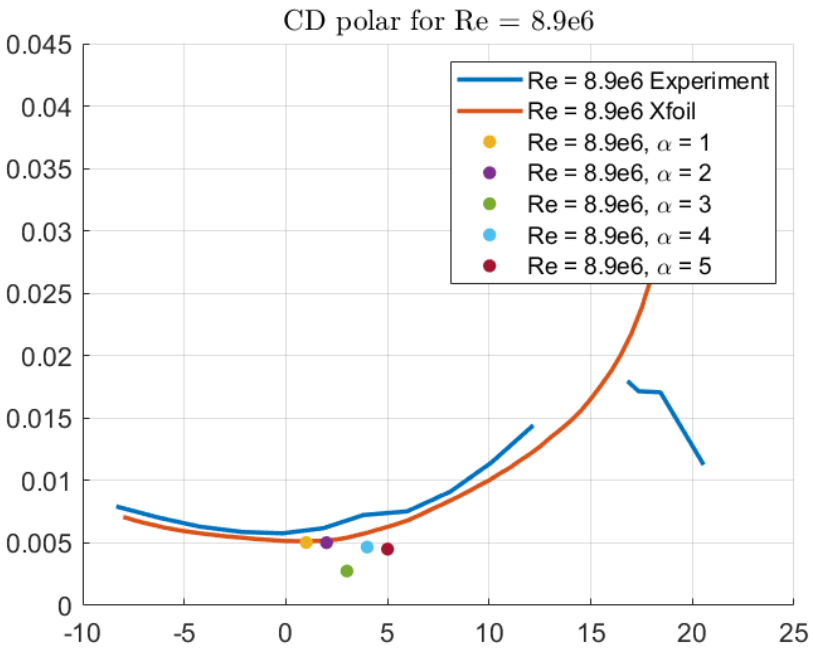

Figure 25: C_d polar for $Re = 8.9 \times 10^6$

A laminar separation bubble at the lower surface was obtained for higher angles of attack, making the panel code ineffective.